Indentation Tests on GaAs: Modelling of the Plastic Zone

R. Lohonka[I,1] , G. Vanderschaeve[I,2] , J. Kratochvíl[II]

[I] *Centre d'élaboration des matériaux et d'études structurales CNRS, B.P. 94347, 31055 Toulouse Cedex France and INSA Toulouse, Physics Departement, 31077 Toulouse Cedex France*

[II] *CTU, Faculty of Civil Engineering, Departement of Physics, Thákurova 7, 166 29 Prague 6, Czech Republic*

ABSTRACT

The stress distribution around an indent is calculated with the help of different analytical elastic solutions — stress fields of Hill, Boussinesq, Mindlin are presented. These stress fields are compared by calculating the shape and dimensions of the plastically deformed region. From it follows that although is the spherical symmetric Hill field quite simple, it describes correctly the plastic zone around Vickers indents in {001} GaAs crystals. Alternatively to the analytical elastic solutions, the stress field is calculated numerically with use of the finite element method. The results are in agreement with electron microscope observations and confirm the suitability of the spherical stress field.

Key words: indentation, stress field tensors, plasticity criterion, finite element method

1 INTRODUCTION

As mentioned in /1/, instrumented indentation has been the subject of rapidly expanding scientific activity and has many possible applications. Indentation at the nanoscopic, microscopic and macroscopic size scales may be used to estimate mechanical characteristics of materials, such as Young's modulus, yield strength, strain hardening exponent and hardness. By the appropriate choice of the indenter shape (i.e. spherical,

---

[1]Present address: Aeronautical Research and Test Institute, Beranovych 130, 199 05 Prague — Letňany, Czech Republic

[2]Corresponding author: tel +33-5622-57885; fax +33-5622-57999; E-mail address: Guy.Vanderschaeve@cemes.fr

conical, Vickers, Berkovich and others), size and applied indentation load, instrumented indentation can be used to probe the properties of surface layers as well as bulk structural materials employed in a broad range of applications. Advances in instrumentation have facilitated very accurate experimental measurements of indentation load as a function of depth of penetration, and computational models for indentation have been reported in recent years /1,2,3,4/.

The dislocation distribution around indents on {001} orientated semiconductors with sphalerite structure has been the subject of a number of investigations /5,6,7,8,9,10/. We will briefly describe the results of observations of /8,9/. To obtain a complex picture of dislocation motion around indentations, the stress field produced by the indenter should be determined. Two approaches are presented. Different elastic solutions expressed in the analytical form are used for calculation of the shape and dimensions of the plastically deformed region. We compare and discuss the obtained results. Another conception is the simulation by finite element method. The plastic zone is then simulated with aid of the Von Mises yielding criterion.

2 DESCRIPTION OF THE EXPERIMENTAL RESULTS

The material studied in /9/ is a n-type GaAs single crystal with carrier concentration of 10^{10} to 10^{12} cm^{-3} and a dislocation density of 10^4 to 10^5 cm^{-2}, grown by the liquid encapsulated Czochralski method. Vickers indentations are achieved at room temperature on the (001) surfaces, the indenter diagonals being parallel to ⟨110⟩ directions. The applied load ranges from 0.049 N to 0.98 N and the dwell time is 15 s /11/. Figure 1 shows the plastic zone around an indent as observed by High Voltage Transmission Electron Microscopy (HVTEM).

In agreement with the predictions of /6/ it consists of:

1. perfect dislocations with Burgers vectors inclined to the surface, which have moved into the crystal on {111} planes which converge beneath the indenter;
2. perfect dislocations with Burgers vectors inclined to the surface which have moved into the crystal on {111} planes which diverge from the indenter;
3. perfect dislocations with Burgers vectors parallel to the surface, which have moved primarily parallel to the surface and outward from the indenter in both ⟨110⟩ directions to form rosettes. In addition, microtwins are observed only in the [110] rosette arm; they are nucleated on — or very close to — the indented surface.

The highly strained region around the impression results from the glide of dislocations with Burgers vector inclined to the surface on the converging and diverging glide systems. On the edges of this zone, dislocations are very straight along the ⟨100⟩ directions which are the projections of inclined ⟨110⟩ directions.

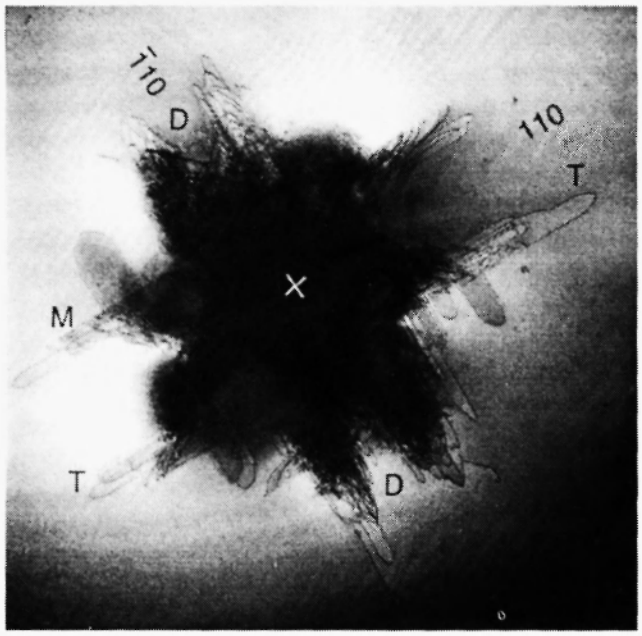

Fig. 1: High Voltage (1MV) TEM image of the plastic zone around an indent performed on GaAs. Bright field micrograph, magnification 7500. The indentation point is marked by cross. T — rosette perfect dislocations, M — microtwins, D — dislocations in the diverging slip planes. Courtesy according to /9/

3 STRESS FIELD MODELING AROUND THE INDENTER

In this section, we summarize four analytical expressions for the elastic stress field which could be suitable for the plastic zone modelling. Presented criterion for the single slip allows to calculate the plastic zone extension and thus determine which result agrees with the experimental observations.

3.1 Analytical expressions for the stress distribution

The stress tensor components are expressed in the spherical coordinates (r,θ,ϕ) except the field of Mindlin for which the cartesian coordinates are used.

The first described kind of analysis is based upon the spherical shell expansion, problem which was solved by Hill /12 /. When a spherical shell with yield strength Y is expanded by inner pressure, and a part of the shell with a radius r_p is deformed plastically, the stress components σ_{rr} and $\sigma_{\theta\theta}$ in the elastic region are written as follows:

$$\sigma_{rr} = -\frac{2Yr_p^3}{3}\left(\frac{1}{r^3} - \frac{1}{r_o^3}\right) \quad (r_p \le r \le r_o), \tag{1}$$

$$\sigma_{\vartheta\vartheta} = \sigma_{\phi\phi} = \frac{Yr_p^3}{3}\left(\frac{1}{2r^3} + \frac{1}{r_o^3}\right) \quad (r_p \le r \le r_o), \tag{2}$$

where r_o denotes the outer radius of the shell.

When the spherical expansion model is applied to the case of indentation of an infinite body, the outer radius r_o can be taken as infinitely large and the last terms in equations (1), (2) can be neglected. We obtain

$$\sigma_{rr} = -\frac{2Yr_p^3}{3r^3} \quad (r_p \le r \ll r_o), \tag{3}$$

$$\sigma_{\vartheta\vartheta} = \sigma_{\phi\phi} = \frac{Yr_p^3}{3r^3} \quad (r_p \le r \ll r_o). \tag{4}$$

By virtue of the symmetry, the state of stress is everywhere a hydrostatic pressure ($\sigma_{\theta\theta}, \sigma_{\theta\theta}, \sigma_{\theta\theta}$) superposed on a uniaxial compression (σ_{rr} -$\sigma_{\theta\theta}$, 0, 0).

Another stress distribution is deduced from Boussinesq /13/. Given a point load P on the flat surface of a semi–infinite half–space, the elastic field is derived as /14 /:

$$\sigma_{rr} = \frac{P}{2\pi r^2}\left[1 - 2\nu - 2(2-\nu)\cos\vartheta\right], \tag{5}$$

$$\sigma_{\vartheta\vartheta} = \frac{P}{2\pi r^2}\frac{(1-2\nu)\cos^2\vartheta}{1+\cos\vartheta}, \tag{6}$$

$$\sigma_{\phi\phi} = \frac{P(1-2\nu)}{2\pi r^2}\left[\cos\vartheta - \frac{1}{1+\cos\vartheta}\right], \tag{7}$$

$$\sigma_{r\vartheta} = P\frac{1-2\nu}{2\pi r^2}\frac{\sin\vartheta\cos\vartheta}{1+\cos\vartheta}, \tag{8}$$

with ν the Poisson's ratio of the indented material. This is the dominant field of a loaded indenter as r increases. There are two regions of positive tensile stress visible in equations (5)–(8). One is σ_{rr} in the surface

($\theta=\pi/2$) which may lead to a ring crack, the other is $\sigma_{\theta\theta} = \sigma_{\phi\phi}$ on the axis ($\theta=0$) where median cracks appear /14/. Note that unlike the Hill stress field the stress tensor contains non diagonal terms. This is also the case for the other stress fields investigated.

Another stress field is of the "blister" type, as described in /14/. The deformed zone beneath the indenter has changed shape and volume, yet is still attached to the elastic half-space. It is therefore equivalent, at a little distance, to a transformed surface inclusion, causing local stresses proportional to $1/r^3$ of the "blister" type, a nucleus of strain situated on a free surface. The field is made by combining a symmetrical centre of pressure with a double force in the z direction /14/. This is equivalent to two outward double forces in the surface plane and an inward double force of equal magnitude normal to it, a combination leaving the surface $z=0$ free of stress. The stress components are /14/:

$$\sigma_{rr} = \frac{\mathfrak{B}}{r^3} 4\left[(5-\nu)\cos^2\vartheta - (2-\nu)\right], \tag{9}$$

$$\sigma_{\vartheta\vartheta} = -\frac{\mathfrak{B}}{r^3} 2(1-2\nu)\cos^2\vartheta, \tag{10}$$

$$\sigma_{\phi\phi} = \frac{\mathfrak{B}}{r^3} 2(1-2\nu)(2-\cos^2\vartheta), \tag{11}$$

$$\sigma_{r\vartheta} = \frac{\mathfrak{B}}{r^3} 4(1+\nu)\sin\vartheta\cos\vartheta. \tag{12}$$

The strength of the field is measured by the constant B. The stresses decrease as $1/r^3$ and therefore contribute nothing at large distances. This stress field is thus a local one, similar to the field of a prismatic dislocation loop. The simple centre of compression is equally localized, and for this reason should not be used to represent the outer elastic field of an indentation. The yielded zone beneath the indenter is assumed to reach the uniform state (the indenter load P is spread as a uniform pressure $p=P/A_c$, where A_c is the indenter's contact area, and the containing pressure normal to this is such that the elastic strain energy density is minimized) and therefore shows no tendency to crack under load.

The last analytical indentation stress field determination is that of Mindlin /15/. A semi-infinite elastic homogeneous solid is considered to be bounded by the plane $z=0$, the positive z axis penetrating into the body. For a point force P applied at point (0,0,0) and acting in the positive z direction, the stress at point (x,y,z) inside the semi-infinite body has the following components:

$$\sigma_{xx} = \frac{Pz}{2\pi r^3}\left[1 - 2\nu - 3\left(\frac{x}{r}\right)^2 - \frac{1-2\nu}{(r+z)^2}\left(r^2 - x^2 + \frac{r}{z}(r^2 - 2x^2)\right)\right], \tag{13}$$

$$\sigma_{yy} = \frac{Pz}{2\pi r^3}\left[1 - 2\nu - 3\left(\frac{y}{r}\right)^2 - \frac{1-2\nu}{(r+z)^2}\left(r^2 - y^2 + \frac{r}{z}(r^2 - 2y^2)\right)\right], \tag{14}$$

$$\sigma_{zz} = -\frac{3Pz^3}{2\pi r^5}, \tag{15}$$

$$\sigma_{xz} = -\frac{3Pxz^2}{2\pi r^5}. \tag{16}$$

Here, $r^2=x^2+y^2+z^2$. The stress field varies as $1/r^2$ as the other presented analytical elastic solutions except the blister field.

3.2 Comparison of analytical stress fields

We compare the above mentioned different stress fields by means of computed shape of plastically deformed region around the indent. Our method is based on the fact that in a single crystal slip generally occurs when the resolved shear stress reaches some critical value called critical resolved shear stress (CRSS) denoted τ_c. The criterion for slip can be written as

$$F = \sigma_{ij} b_j n_i \geq \tau_c b, \tag{17}$$

where F is the glide component of the Peach–Koehler force determining the acting of the external stress field with components σ_{ij} on dislocation segment with a unit length, n_i are components of the unit vector normal to the slip plane, b_i components of its Burgers vector. For a given stress field and dislocation segment equation (17) yields the distance r_c at which the resolved shear stress reaches the value of CRSS. We assume that this distance bounds the plastically deformed region.

To compare the shape and dimensions of the plastic zone obtained by means of different stress fields, we take into account the glide plane with normal $\vec{n}$ =[111] and there perfect dislocations with Burgers vectors $\vec{b}$ =1/2[1$\bar{1}$0], representing the rosette dislocations. This choice is justified by the fact that the calculated shape of the plastic zone is directly comparable with the observed one. However, the calculation can proceed with arbitrary glide system and its perfect or partial dislocations, only the comparison with the observation is not so straightforward.

Parameters used in the calculations are resumed in Table 1. The strength of the blister field B is estimated as $B=0.05pa^3$, with the pressure $p=P/A_c$=5250 MPa /11/, and a=2.1 μm is the radius of the zone under indenter which we suppose to delimit the nucleus of blister strain. The value of the constant B hangs together with character of observed cracks and a detailed analysis can be found in /14/.

Note that all graphs show the absolute value of the computed radius r_c for different cases. The particularity of the Mindlin's stress field (13)–(16) is that it realistically describes the unstressed surface of the sample. To obtain the surface contour, the limit of r for angle tending to $\pi/2$ is used.

Table 1

Parameters used in the calculation of the dimensions and shape of the plastic zone obtained by indentation of GaAs single crystals /11/.

Poisson's ratio	ν = 1/3
CRSS /16/	τ_c=800 MPa
yield strength /16/	Y=1700 MPa
radius of plastically deformed zone /11/	r_p=5 μm
indentation load /11/	P=0.049 N
B (blister field, estimated)	$B=2.6\cdot10^{-9}$ Nm

Figure 2 presents the shapes of the plastic zone on the indented surface calculated with above presented stress tensors for the slip system 1/2 [1$\bar{1}$0] (111) forming rosettes.

The spatial extension of the plastic zone obtained for this system with the Hill's stress field is shown in Figure 3. We will discuss the results in section 4.

3.3 Elastic indentation stress field determined by the finite element method

Alternatively to the different analytical solutions, the stress field distribution around an indent can be calculated numerically. We used the finite element system ABAQUS/Explicit. The plastic zone is then determined with help of the Von Mises yield criterion.

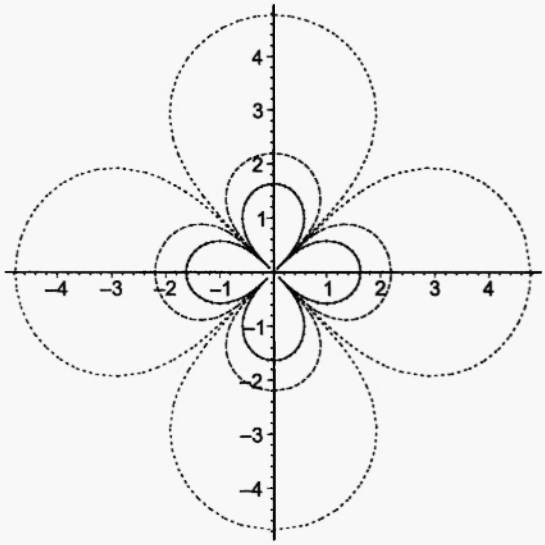

Fig. 2: Calculated shapes of the plastic zone on the indented surface for the slip system 1/2 $[1\bar{1}0](111)$. The largest zone is that of Hill (dash-dotted line) followed by blister field (dashed line), Boussinesq (solid line) and Mindlin (points) stress tensors lead to the same result. Dimensions are in micrometers.

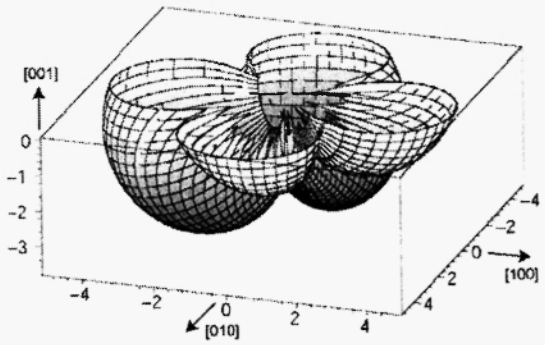

Fig. 3: Extension of the plastic zone calculated with the Hill's stress field for the slip system $1/2[1\bar{1}0](111)$. Dimensions are in micrometers.

Because of the symmetry of the Vickers indenter only 1/4 of the indented sample is considered. The dimensions of the finite element part and the experimental sample are the same to enable a direct comparison of calculated and experimental results. The segment corresponding to the indenter pressed into the surface is removed, the calculation conditions thus represent the phase before removing of the indenter from the

sample. The penetration depth of the Vickers pyramid is determined from the dimensions of obtained indenter imprint considering that there was no back response of the material after the indenter removing, i.e. rigidity of the sample after penetration of the indenter is supposed.

The material behaviour of the sample was chosen to be elastic and anisotropic with elastic moduli presented in Table 2.

The FEM mesh consists of 4-node linear tetrahedra and 8-node linear bricks. In the boundary conditions the applied force and its contact surface is defined, lateral sides are fixed. Figure 4 shows the obtained Von Mises stress distribution with the maximal value corresponding to the elasticity limit of the material.

It can be concluded that dislocations will preferentially nucleate close to the edges of indenter in the volume of crystal. Also the directions of the rosette arms extensions are in agreement with observations.

Table 2

GaAs material parameters used in the FEM calculation of the dimensions and shape of the indentation induced plastic zone.

elastic moduli	$C_{11}=11.81\times10^{10}$ Pa
	$C_{12}=5.32\times10^{10}$ Pa
	$C_{44}=5.92\times10^{10}$ Pa
GaAs density	$\rho_{GaAs}=5317$ kgm^{-3}

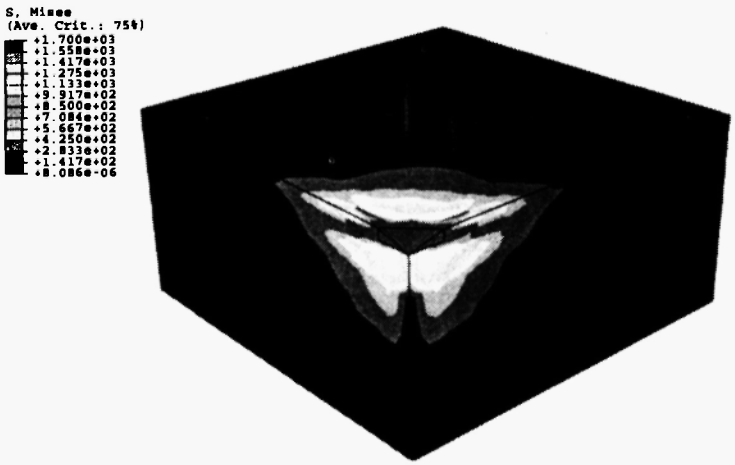

Fig. 4: Von Mises stress calculated with ABAQUS/Explicit. Stress in MPa. The highest stress value corresponds to the compression yield stress.

4 DISCUSSION OF THE RESULTS

We analyze the obtained results (Figures 2, 3, 4) with respect to the observed situation (Figure 1) and conclude which expression for the stress tensor seems us the best.

All calculated shapes of the plastic zone on the indented surface are similar, two of them (that of Boussinesq and Mindlin) even the same. The dimensions of the plastic zone corresponds in the case of Hill's stress tensor to the observed extension, the length of the arms at the surface equals to 4.4 μm. This agreement is due to the term r_p=5 μm which introduces directly the experimental dimensions of the plastic part into the stress tensor. Such a term is not present in the other stress field expressions, however in the case of the Boussinesq and Mindlin field it is possible to correct the dimensions of the plastic zone by introduction of the strength factor as is B in the blister stress tensor.

When the position of the indenter is sketched, as done in Figure 5, it is seen that the force acting on the rosette system equals to zero along the indenter's diagonals. However, the concentration of the stress is elevated enough for crack nucleation. The extension of the plastic zone results from the combination of dislocation nucleation in the vicinity of indenter and their propagation in the glide planes. Dislocations are not observed in the place of maximal calculated stresses on the x and y axis because the corresponding potential nucleation locality is too far from the indenter: indeed dislocations are gliding on {111} planes whose traces on the (001) surface are along ⟨110⟩ directions. However it is troublesome to predict such a complex dynamic process by virtue of the elastic stress distribution.

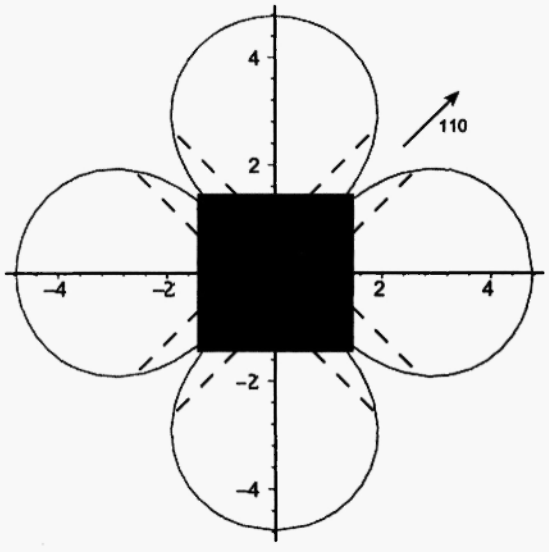

Fig. 5: Calculated extension of the rosettes on the surface with the stress field of Hill. The indenter position and the observed directions of rosette perfect dislocations are sketched. Dimensions are in micrometers.

From the spatial Hill's stress distribution (Figure 3) it can be concluded that the maximal extension of the dislocations can be expected in the volume of the crystal at about 1 μm under the indented surface. This is seen for the parts along the $[0\bar{1}0]$ and $[\bar{1}00]$ directions. This is consistent with TEM observations: indeed the elongated hairpin shape of rosette dislocations strongly suggests that they are formed deeply in the crystal /9/. The extension of the two other parts is maximal at the surface, the part in the crystal is shallower. This asymmetry is due to the glide system (111) considered. In the upper halfspace delimited by the axis [110], i.e. the parts along the $[0\bar{1}0]$ and $[\bar{1}00]$ directions, the plane (111) is converging under the indenter, whereas for the parts along [100] and [010] directions the plane (111) is diverging. The penetration of the plastic zone into the sample is limited. This is not so in the case of the Boussinesq's and Mindlin's tensors, where the plastic zone goes very deep into the crystal because of the term $1/(1+\cos\theta)$ causing singularity for $\theta=\pi$. The elevated values of stress along the z-axis do not necessarily involve the presence of dislocations which nucleate in the vicinity of indenter. Their propagation on converging planes leads to formation of locks. The depth reached by dislocations gliding into the crystal is thus limited. Another possibility is the dislocation nucleation in the bulk but the stresses are not high enough to induce such a process.

From the numerical calculations it follows that the most important stress concentrations are near the edges of the indentor, under the surface. The distribution of the Von Mises stress hints the extension of the plastic zone which is comparable to the results obtained by use of the different analytical stress fields and the criterion (17). The direct comparison of the calculations with experiments is possible in the case of rosette dislocations where the propagation directions are clearly seen. Nevertheless, from the calculated stress distribution dislocation glide under the indenter can be reasoned as well.

5 CONCLUSION

Four different analytical expressions that seemed suitable as a model of the stress field around the Vickers indenter were introduced. The comparison is based on the calculation of the shape and dimensions of the plastic zone defined by equation (17). Since the results obtained for rosettes with each stress tensor are similar, it is concluded that even the simple and from the calculation point of view unpretending spherical Hill stress field approaches the experimentally obtained result quite well. Note that Yoshioka in his investigation of indented Si single crystals /17/ also concluded that the stress distribution could be considered as nearly spherical, although the plastic zone is far from it.

Finite element calculation of the stress field around Vickers indent confirms the results obtained with the analytical expressions for the stress tensor. The plastic zone extension is consistent with the HVTEM observations. They estimate well the result of complicated processes involving dislocations only working with the stress and geometry of the slip systems.

REFERENCES

1. S. Suresh and A.E. Giannakopoulos, Deformation and properties of homogeneous and graded surfaces: Theories and experiments involving depth–sensing indentation, Proc. of the 20th Risø International Symposium on Materials Science *Deformation-Induced Microstructures: Analysis and Relation to Properties.*, Editors: J. B. Bilde Sørensen, J. V. Carstensen, N. Hansen, D. Juul Jensen, T. Leffers, W. Pantleon, O. B. Pedersen and G. Winkler, Risø National Laboratory, Roskilde, Denmark, pp. 183–200, 1999.
2. M. Fivel, M. Verdier and G. Canova, 3D simulation of a nanoindentation test at a mesoscopic scale, *Mat. Sci .Eng. A*, **923**, 234–236 (1997).
3. M.C. Fivel, C.F. Robertson, G.R. Canova and L. Boulanger, Three–dimensional modeling of indent–induced plastic zone at a mesoscale, *Acta Mater.*, **46**, 6183–6194 (1998).
4. H.S. Leipner, D. Lorenz, A. Zeckzer, H. Lei and P. Grau, Nanoindentation pop-in effect in semiconductors, *Physica B*, **446**, 308–310 (2001).
5. H.R. Höche and J. Schreiber, Anisotropic deformation behaviour of GaAs, *Phys. Stat. Sol.(a)*, **86**, 229–236 (1984).
6. S.G. Roberts, P.D. Warren and P.B. Hirsch, Knoop hardness anisotropy on {001} faces of germanium and gallium arsenide, *J. Mater. Res.*, **1**, 162–176 (1986).
7. P.B. Hirsch, P. Pirouz, S.G. Roberts and P.D. Warren, Indentation plasticity and polarity of hardness on {111} faces of GaAs, *Phil. Mag. B*, **52**, 759–784 (1985).
8. S. Koubaïti, C. Levade, G. Vanderschaeve and J.J. Couderc, Vickers indentation on the {001} faces of GaAs under infrared illumination and in darkness, *Phil. Mag. A*, **80**, 83–104 (2000).
9. C. Levade and G. Vanderschaeve, Rosette microstructure in indented (001) GaAs single crystals and the alpha/beta assymetry, *Phys. Stat. Sol.(a)*, **171**, 83–88 (1999).
10. E. Le Bourhis and G. Patriarche, Plastic deformation of III–V semiconductors under concentrated load, *Prog. Crystal Growth and Charact.*, **47**, 1–43 (2003).
11. S. Koubaïti, Ph.D. Thesis, I.N.S.A. Toulouse, 1996.
12. R. Hill, *The Mathematical Theory of Plasticity*, Oxford University Press, London, 1950.
13. J. Boussinesq, *Application des potentiels à l'etude de l'equilibre et du mouvement des solides elastiques*, Gauthier–Villars, Paris, 1885.
14. E.H. Yoffe, Elastic stress field caused by indenting brittle materials, *Phil. Mag. A*, **46**, 617–628 (1982).
15. R.D. Mindlin, Force at a point in the interior of a semi–infinite solid, *Physics* **7**, 195–202 (1936).
16. Y. Androussi, G. Vanderschaeve and A. Lefebvre, Slip and twinning in high–stress–deformed GaAs and the influence of doping, *Phil. Mag. A*, **59**, 1189–1204 (1989).
17. M. Yoshioka, M., Plastically deformed region around indentations on Si single crystal, *J. Appl. Phys.*, **76**, 7790–7796 (1994).